

Frank P. Bierlein · Finbarr C. Murphy ·
Roberto F. Weinberg · Terry Lees

Distribution of orogenic gold deposits in relation to fault zones and gravity gradients: targeting tools applied to the Eastern Goldfields, Yilgarn Craton, Western Australia

Received: 28 October 2005 / Accepted: 6 December 2005
© Springer-Verlag 2006

Abstract A quantitative spatial analysis of mineral deposit distributions in relation to their proximity to a variety of structural elements is used to define parameters that can influence metal endowment, deposit location and the resource potential of a region. Using orogenic gold deposits as an example, geostatistical techniques are applied in a geographic-information-systems-based regional-scale analysis in the high-data-density Yilgarn Craton of Western Australia. Metal endowment (gold production and gold ‘rank’ per square kilometer) is measured in incremental buffer regions created in relation to vector lines, such as faults. The greatest metal tonnages are related to intersections of major faults with regional anticlines and to fault jogs, particularly those of dilatant geometry. Using fault length in parameter search, there is a strong association between crustal-scale shear zones/faults and deposits. Nonetheless, it is the small-scale faults that are marginal or peripheral to the larger-scale features that are more prospective. Gravity gradients (depicted as multiscale

edges or gravity ‘worms’) show a clear association to faults that host gold deposits. Long wavelength/long strikelength edges, interpreted as dominantly fault-related, have greater metal endowment and provide a first-order area selection filter for exploration, particularly in areas of poor exposure. Statistical analysis of fault, fold and gravity gradient patterns mainly affirms empirical exploration criteria for orogenic gold deposits, such as associations with crustal-scale faults, anticlinal hinge zones, dilational jogs, elevated fault roughness, strong rheological contrasts and medium metamorphic grade rocks. The presence and concurrence of these parameters determine the metallogenic endowment of a given fault system and segments within the system. By quantifying such parameters, the search area for exploration can be significantly reduced by an order of magnitude, while increasing the chance of discovery.

Keywords Geographic information systems · Orogenic gold · Yilgarn Craton · Gravity gradients · Multiscale edges · Exploration criteria · Prospectivity analysis

Editorial handling: R. Goldfarb

F. P. Bierlein · R. F. Weinberg · T. Lees
pmd*CRC, School of Geosciences, Monash University,
P.O. Box 28E, Melbourne, VIC 3800, Australia

F. P. Bierlein (✉)
TSRC and CET,
School of Earth and Geographical Sciences,
University of Western Australia,
35 Stirling Highway,
Crawley, WA 6009, Australia
e-mail: fbierlein@tsrc.uwa.edu.au
Tel.: +61-8-64887846
Fax: +61-8-64881090

F. C. Murphy
pmd*CRC, School of Earth Sciences,
University of Melbourne,
Melbourne, VIC 3010, Australia

Present address:

T. Lees
Copper Strike Limited,
Level 9, 356 Collins Street,
Melbourne, VIC 3000, Australia

Introduction

Many hydrothermal mineral deposit types display a spatial relationship with faults and crustal discontinuities (e.g., Groves et al. 1998; Sillitoe 2000; Betts and Lister 2002; Haynes 2002; Grauch et al. 2003). Economic geologists have long recognized an empirical relationship between ore deposits and major structures or fault corridors. Such features are likely to play an important role in providing pathways for focusing fluids into the upper crust and may be described in terms of translithospheric columns of low strength and high permeability (e.g., Cox et al. 2001; Chernicoff et al. 2002). This spatial association with major faults has been successfully used as a guide in exploration (e.g., Olympic Dam; Haynes 2002). On the other hand, not every major fault is metallogenically well-endowed, and many first-order faults appear to contain little or no

hydrothermal mineralization. Examples include the Mesozoic Gowk Fault (Walker and Jackson 2002), the Palaeozoic South Armorican Shear Zone (Jegouzo 1980), the Palaeoproterozoic Cloncurry Overthrust (Drummond et al. 1998) and the Archaean Mount Monger Fault (Goleby et al. 2002). Distinguishing what faults are important for mineralization is a key exploration uncertainty; thus, we have attempted to quantify fault-related parameters that may subsequently be used to contribute towards improving mineral discovery. Exclusive of physical process modelling (e.g., Ord and Hobbs 1989; Holyland and Ojala 1997; Oliver 2001) and studies of geometrical and geophysical parameters (e.g., Knox-Robinson and Groves 1997; Brown et al. 2000; Knox-Robinson 2000), there are few studies to systematically test empirical exploration parameters in regional-scale data sets. The analysis of such parameters may provide clues as to why certain lithospheric-scale fault systems and corridors are metallogenically well-endowed, whereas other seemingly identical faults are barren.

An assessment of the geometry of metallogenically well-endowed fault systems and corridors in a global context suggests that many are highly non-planar (e.g., Blenkinsop and Bierlein 2004; Weinberg et al. 2004), with associated ‘damage zones’ that record a complex reactivation history (Sibson 2001). Such fault systems tend to be subvertical at shallow crustal levels, but are commonly interpreted to have a listric geometry at greater depths (e.g., Goleby et al. 2004). This has implications for their capability to transect the lithosphere and penetrate into the asthenosphere, thus tapping mantle-derived fluid reservoirs. Other aspects of relevance to the metal endowment of faults include the presence of complex lithostratigraphic sequences with strong rheological contrasts promoting strain partitioning (Cox et al. 2001), proximity to ancient continental margins and suture zones (Robert and Poulsen 2001), the presence of mafic to intermediate igneous rocks (providing a possible link to asthenospheric input; Rock et al. 1990; Bierlein et al. 2001), extensive alteration resulting from the advective/convective throughput of large fluid volumes and geometric aspects that include far-field orientation, fault ‘misalignment’ and length, and the nature of displacement and relay zones between fault segments (Cowie and Scholz 1992; Groves et al. 1998; Goldfarb et al. 2001; Peacock 2003).

Many of the abovelisted parameters are empirical or are based on modelling scenarios that require systematic testing. In this study, we attempt to quantify some of these interpretations using public domain digital geology and processed gravity data. Specifically, this research is aimed at: (1) distinguishing mineralized from non-mineralized fault systems, and (2) constraining the spatial relationship between gold deposits and controlling structures and thus is ultimately directed towards improving confidence in area selection decisions made by explorationists.

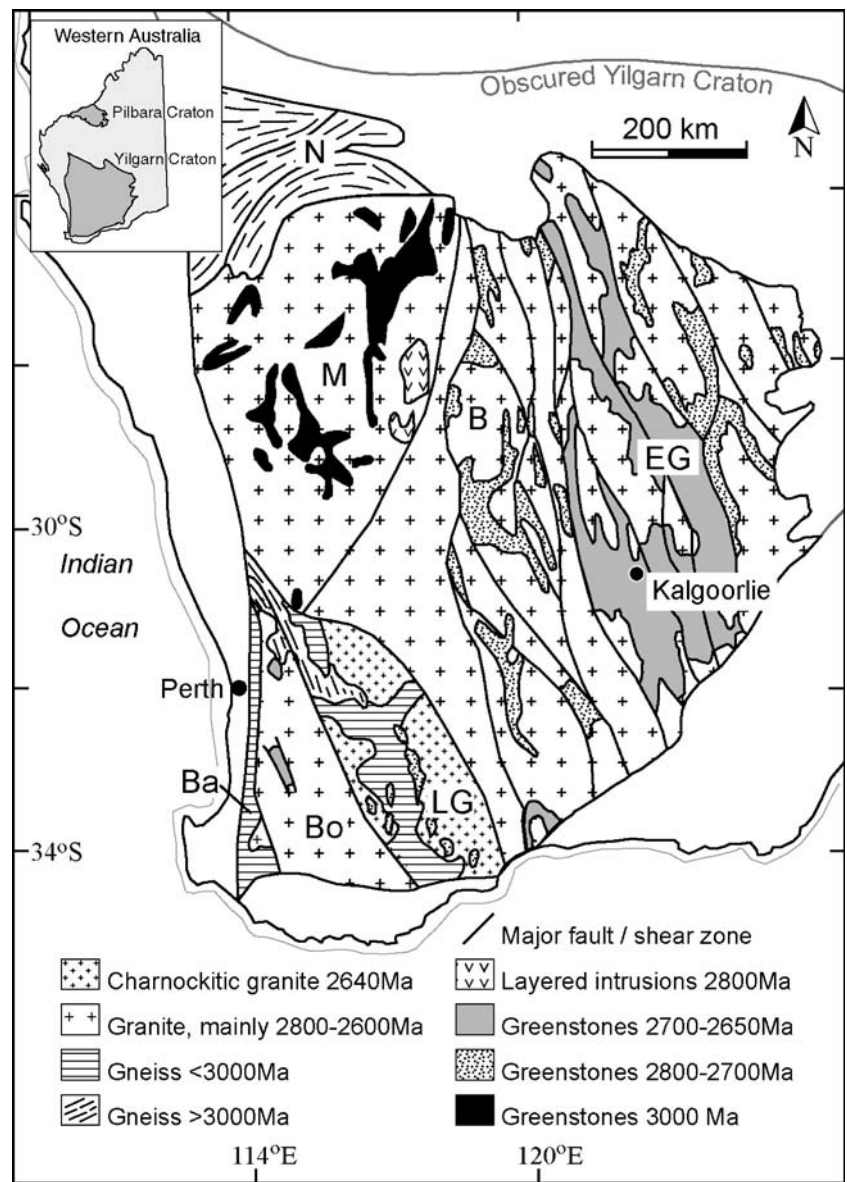
A multidisciplinary approach to prospectivity analysis: methodology and data input

Several recent studies have highlighted the benefit of integrating multifaceted data sets in order to constrain the metallogenesis of a region and its relationship with large-scale fault structures, particularly where the origin of the mineral deposits is controversial and/or is associated with crustal structures that are obscure. For example, Crafford and Grauch (2002) used geological, geophysical and isotopic data to suggest a fundamental link between the location of world-class Carlin gold deposits and concealed deep crustal fault zones in northcentral Nevada. Vos et al. (2004) established linkages between orogenic gold deposits and concealed crustal breaks using a combination of structural–tectonic, geophysical and geochronological data in northeastern Queensland. These authors also used multiscale edge analysis and forward modelling to reinterpret the depth extent and tectonic evolution of a poorly defined first-order fault in this region, and demonstrated the control of these parameters on variations in mineral endowment along the fault. In this paper, we take a multifaceted approach in examining some conceptual models of structural controls on orogenic gold deposits in the Yilgarn Craton (Fig. 1) and apply parameter search using regional geological and geophysical data. An assumption built into this analysis is that the pattern of structures we currently see at this regional scale of analysis also existed at the time of mineralization. While this is unlikely to be valid in detail, the late stage of mineralization in the geological evolution of the terrain provides some bases for that assumption (e.g., Groves et al. 2000).

To determine which faults might extend to the greatest depth, we use strikelength as a loose proxy for down-dip extent as, intuitively, long strikelength faults are more penetrative than are short faults. The former perhaps offers increased potential for tapping ore-bearing fluids and provides more permeable pathways via wider damage zones for focusing such fluids. Yet, counterintuitively, at the orebody scale, small faults can frequently appear important in the localization of mineralization. Our analysis, therefore, includes mapped fault populations and their related gravity gradients over a range of scales, down to an approximately 1-km strikelength cutoff. From these data, we derived parameters that are relevant to mineral exploration and applicable at regional and prospective scales in the Yilgarn Craton.

Faults are commonly associated with potential field gradients, particularly where rocks of contrasting densities and/or magnetic susceptibilities are juxtaposed. Yet not all gradients are necessarily fault-induced. Establishing a connection between fault-controlled mineral deposits and potential field gradients has important consequences when exploring in undercover areas (e.g., O’Driscoll 1990; Russell and Haszeldine 1992; Betts et al. 2004; Stephens et al. 2004). The relationship of regional-scale to continental-scale discontinuities to mineralization in a geodynamic context was highlighted by Hobbs et al. (2000), who drew attention to a deep-seated gravity gradient in northern

Fig. 1 Major geological components of the Yilgarn Craton, Western Australia. Identified terranes: *B* Barlee, *Ba* Balingup, *Bo* Boddington, *EG* Eastern Goldfields, *LG* Lake Grace, *M* Murchison, *N* Narryer (adapted from Myers 1995; Wilde et al. 1996)



Australia (the Barramundi ‘worm’; see below) and the proximity of world-class Proterozoic massive sulphide deposits (Mt. Isa, Century, HYC). Similarly, Archibald et al. (2001) noted a correlation between major gravity gradients in Australia and the locations of large Zn–Pb deposits and, to a lesser degree, of major Cu deposits.

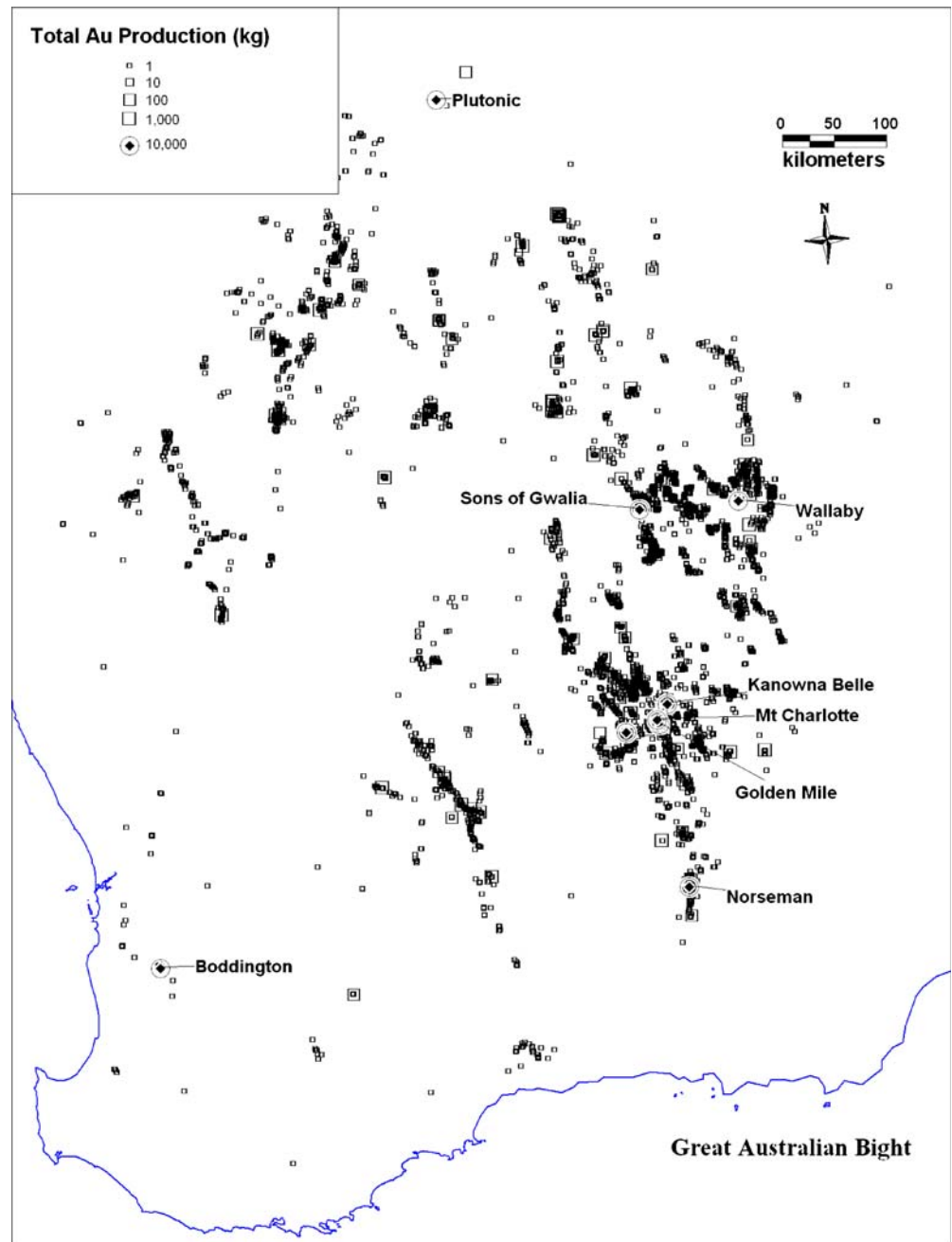
Input data for the present study are existing gold deposits, mapped and interpreted faults, and multiscale gravity gradients. The spatial coherence of these essentially 1-D, 2-D and 3-D data sets, respectively, is investigated in a geographic-information-systems (GIS)-based geostatistical analysis, with the goal of reducing search area while improving the chance of discovery.

Mineral deposit data (Fig. 2) were derived from the Australian Mineral Occurrences Database (MINLOC; Ewers et al. 2002a) and the Australian Mineral Deposits Database (OZMIN; Ewers et al. 2002b). We treat gold occurrences as a single ‘orogenic-type’ deposit for the purposes of this analysis while recognizing that there may

be a range of deposit styles. Such an assumption is valid because this deposit type is, by far, the most dominant gold deposit type in the studied craton. These were first filtered to remove duplicates and non-gold occurrences, and the remaining 9,905 occurrences were numerically classified (1–5 scale) according to relative deposit size (i.e., total contained gold): 1 occurrence or <10 kg; 2 10–100 kg; 3 100–1,000 kg; 4 1,000–10,000 kg; and 5 >10,000 kg of Au. Of the 9,905 occurrences, the 152 largest deposits produced a total of 6,247 t of Au. The classification system was applied simply to take into account the numerous occurrences without reported production.

The second parameter was that of fault (Fig. 3) and fold trends, which was derived from the Geological Survey of Western Australia digital coverage (<http://www.doir.wa.gov.au>). This data set comprises a combination of mapped and inferred faults, as interpreted from both regional aeromagnetic and/or gravity data. Processing of these data involved extraction of duplicate lines and joining of

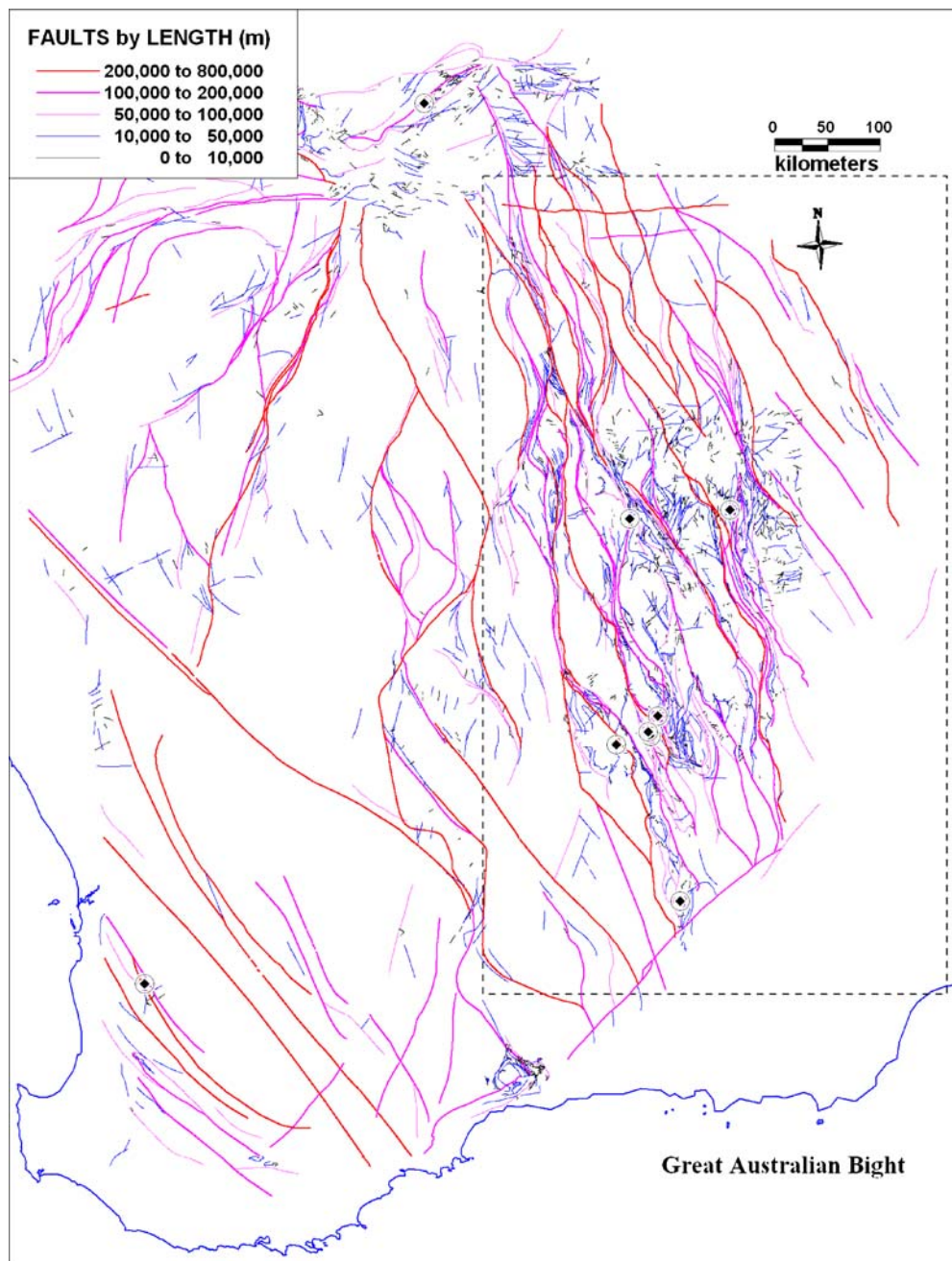
Fig. 2 Distribution of gold deposits in the Yilgarn Craton, ranked by production size (in kg)



contiguous line segments (concatenation). The degree of linkage of faults was determined by visual interpretation; from this, individual fault lengths were computed (Fig. 3). Determinations of where one fault ends and another begins are highly subjective, particularly given the nature and scale of the data. We have sought to define a coherent geometry of interconnected faults so as to emphasize the through-going nature of major fault systems. The major trends are north-striking and northwest-striking structures that define the main geological domains, and there are also subsidiary northeast-trending and east-northeast-trending cross-faults.

The third data parameter is regional-scale gravity (Fig. 4; from Geoscience Australia (<http://www.ga.gov.au/minerals/index.html>)). The traditional interpretation of a 2-D geophysical image essentially involves tracing a contact or edge between bodies of contrasting density or magnetic susceptibility, separating the highs and the lows. Filters, sun angles and upward continuations are typically introduced to enhance the image. A critical aspect of the interpretation is determining the near-surface positions of maximum gradient in the data. A limitation, however, is that the mapped position of the gradient by one person—and perhaps its geological meaning—may differ from that

Fig. 3 Simplified map of the Yilgarn Craton, showing the location of mapped and inferred faults (coloured by strikelength) and major gold deposits. *Inset:* box shows region of gravity data (Fig. 4)

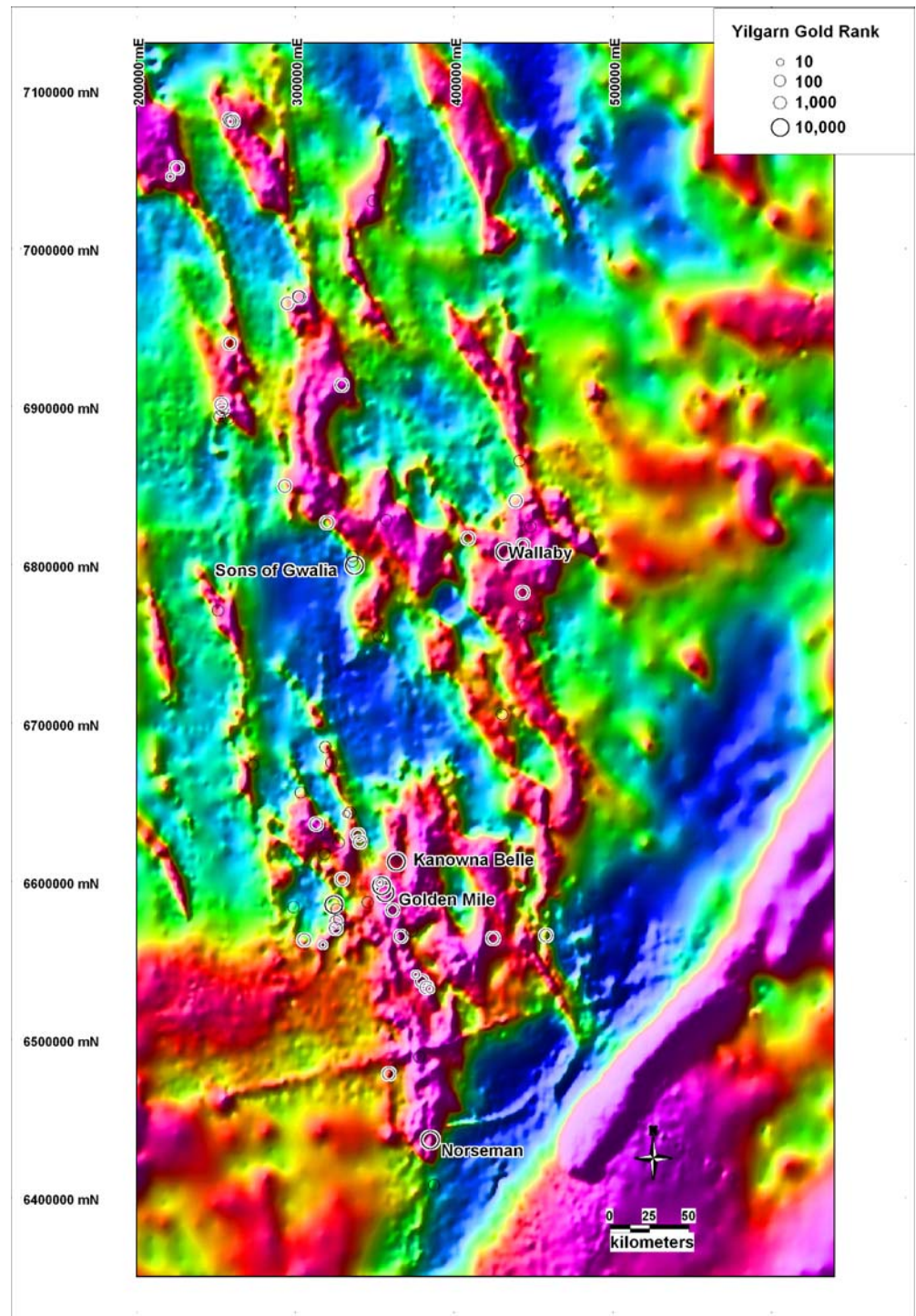


of the next person, with thus the eye of the beholder being a key factor in ambiguity. As exploration is conducted in the near-surface or, at most, shallow depths, there can be costs associated with this uncertainty in position. To address this, the ‘worming’ technique (e.g., Hornby et al. 1999) is applied to automatically detect the positions and strengths of gradients.

This technique yields a 3-D spatial representation of the gradients, through a mathematical process of wavelet-based transformation of gridded data at successive upward continued (aboveground) heights (Archibald et al. 1999; Hornby et al. 1999). This provides information on the apparent dip direction and the lateral and depth persistence of contacts that have a detectable density contrast across

them, and it reduces bias in determining the position of gradients. The procedure has been optimized by Fractal Graphics (now Geoinformatics) using FracWormer™. Gravity gradient points are visualized as 3-D arrays over successive heights of upward continuation (Fig. 5; Archibald et al. 1999). When visualized over a range of scales, the points appear to coalesce into ‘sheets’ that can have an intuitive geological appeal. The terms ‘fine-scale’ (i.e., high-frequency/low-level) and ‘coarse-scale’ (i.e., low-frequency/high-level) edge sheets refer to the height to which the individual gradient can be detected; this is a function of individual geological boundaries. Contacts with no density contrast across them are not detected by the ‘worming’ process, but some such boundaries (e.g.,

Fig. 4 Bouguer gravity image of the eastern Yilgarn Craton showing the location of major gold deposits [ranked by production of gold (in t)] (image produced by Indrajit Roy, Geoscience Australia, with permission)



cross-faults) may be inferred through linear truncations and offsets in subjacent gravity gradient sheets. With some exceptions, coarse-scale gradient sheets generally relate to deeper-level and more persistent geological contrasts, such as those across major fault contacts. Gravity data are generally more useful in this regard than magnetic data. Synthetic modelling indicates that the dip direction of a gravity gradient sheet can mirror a geological contact (e.g., folds, faults and intrusive bodies; Fig. 5) up to the amplitude (w) maxima (Holden et al. 2000). Using the

height and length persistence of gravity gradient sheets, inferences can be made about the relative dimensions of geological boundaries (Murphy et al. 2004).

Yilgarn gravity data were processed to an upward continuation of 60 km using *FracWormer*TM and yield information on geological contacts that may persist into the lower crust (approximately 30 km). From this, a regional map of the gravity gradient point data that are colour-coded by the height of upward continuation (z) and a range of fine-scale to coarse-scale gradient sheets may

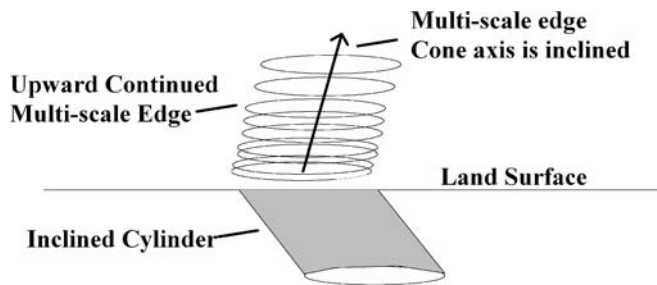


Fig. 5 2-D visualisation of synthetic multiscale edges (*gravity gradients*) due to an inclined cylinder; note the inclined gravity gradient sheet mirrors the dip of the cylinder and the amplitude (w) of the gradient increases with height towards a maxima (modified from Archibald et al. 1999)

be constructed (Fig. 6). Postprocessing of the 3-D data set (using Geoscope software; <http://www.graticule.com/products/MapServer5Turbo.html>) involves derivation of a map that represents near-surface gradients in terms of their total height intensity. This is achieved by applying a nearest-neighbour algorithm across successive height levels (z) so that near-surface points are attributed with the maximum height of the associated gravity gradient sheet (z_{wt}). We use near-surface gradient points (Fig. 6, blue lines) as the level to which all other upward continued levels are projected. Further processing steps involve conversion of gradient points to vector lines, which allows investigation of gradient height, strikelength, trend and straightness parameters. This provides the interpreter with additional constraints with which to model geological sources.

Regional-scale intensity images of height and length, respectively, are derived from vectorized gravity gradients (Figs. 7 and 8). There is a relative coherence between these two parameters (i.e., many long strikelength edges persist to high levels of upward continuation, suggesting greater depth persistence). These imaged data are derived from resolving the strike coherence, continuity and connectivity of vector lines and involve joining contiguous features (concatenation) from which the length parameter is derived. The exact geological source of each gravity gradient edge has not been determined in the current analysis, being that this is solely a first-pass approach to understanding the nature of the gradients. Notwithstanding the limitation of using a geologically ‘mixed’ population of gradients (i.e., gravity edges related to a range of geological contacts), the approach perhaps benefits by reducing interpretation bias in utilizing the full range of gradients, rather than a priori selecting those that necessarily relate to faults.

Gold and shear zones in the Eastern Goldfields Province, Yilgarn Craton

The relationship between orogenic gold deposits and shear zones has been a major focus for both exploration and research. Detailed mapping and high-quality regional aeromagnetic imagery have led to the generation of maps

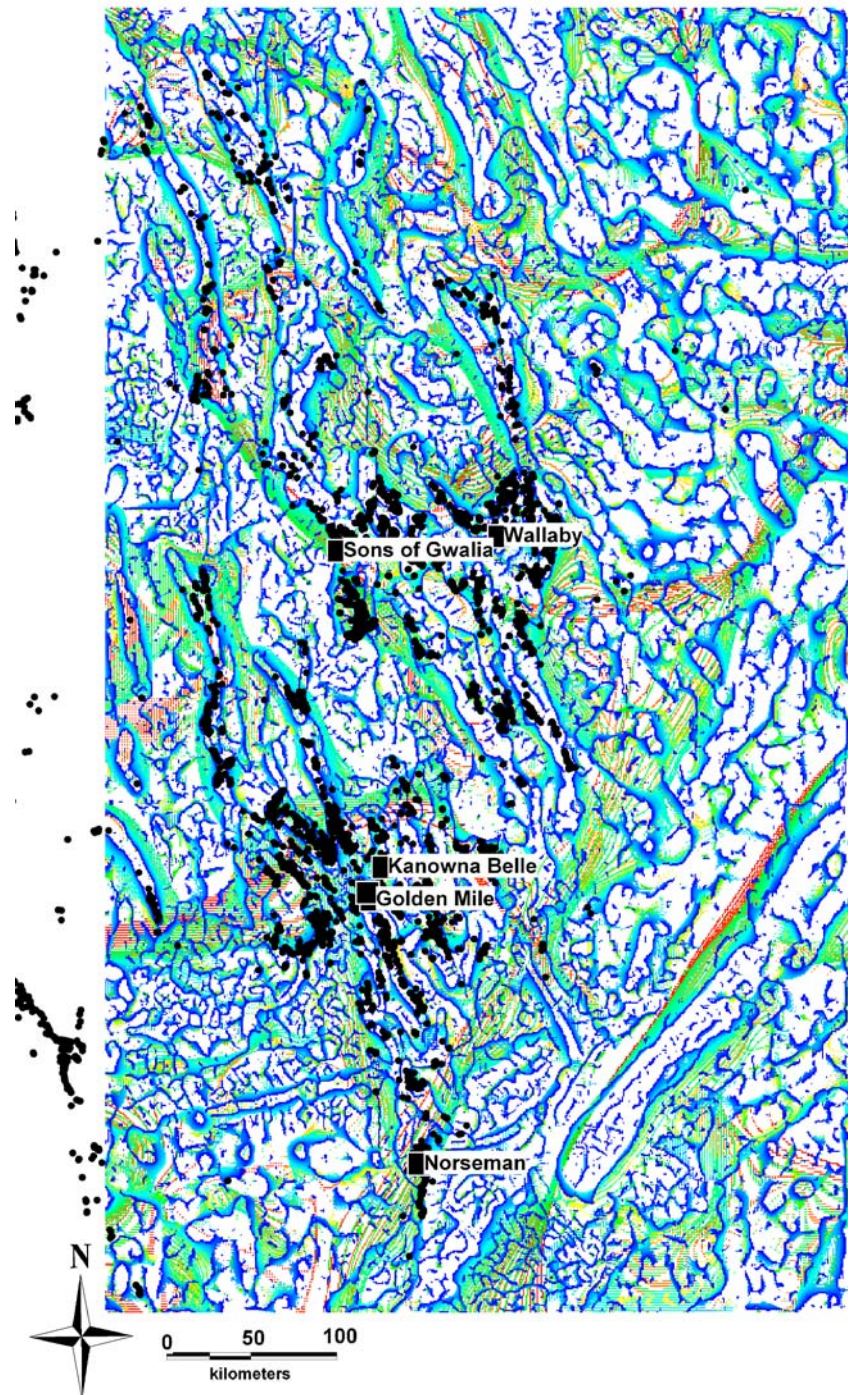
showing shear zones in the poorly exposed Yilgarn Craton (Fig. 3). Such data have been used in a number of ways to investigate the spatial relationship between shear zones and gold deposits. Gold camps are commonly related to jogs in the main trends of regionally important shear zones (Cox and Ruming 2004; Micklethwaite and Cox 2004; Weinberg et al. 2004).

Weinberg et al. (2004) investigated the spatial relationship between gold camps and jogs along the main trend of the Boulder–Lefroy Shear Zone using digital 1:500,000 maps. This is the most endowed shear zone in the Eastern Goldfields and controls four world-class gold camps (>100 t of contained gold), including the giant ~2,000-t Au Golden Mile deposit in Kalgoorlie. An extraordinary feature of these deposits is that they are regularly spaced along the strike of the shear zone at intervals of 35 ± 5 km. Weinberg et al. (2004) investigated whether major changes in the trend of the shear zone are related to areas of gold deposition; thus, they used a small-scale map to avoid local ‘noise’.

The Boulder–Lefroy Shear Zone is a 200-km-long lineament trending north/northwest to south/southeast, which traverses a folded sequence of rocks that includes komatiites, basalts, felsic volcanoclastic rocks, mafic–ultramafic sills and felsic intrusions, generally porphyritic dykes. The shear zone developed initially as a number of thrusts during the D_2 regional crustal thickening event (Weinberg et al. 2005). Thrusts were reactivated and connected via jogs during a later sinistral shearing event (D_3), which was responsible for the present trend of the shear zone and its irregularities. The D_3 shearing was later overprinted by D_4 brittle faulting, which gave rise to north/northeast-trending dextral faults that cut and displace the Boulder–Lefroy Shear Zone. Gold was deposited along the shear zone during D_3 , with the exception of the Golden Mile where gold was most likely deposited during both D_2 and D_3 deformation (Weinberg et al. 2005). Weinberg et al. (2004) found that the regular distribution of gold camps is associated with regional jogs in the trend of the Boulder–Lefroy Shear Zone. Dilation during D_3 sinistral shearing caused development of counterclockwise jogs (low azimuth values) that became well-endowed areas, whereas areas with no significant dilational jogs are considerably less well-endowed. However, in several places (e.g., St. Ives goldfield), the deposits are not located within dilational segments and instead are concentrated in low-displacement faults and shear zones that are several kilometers away from the jogs.

Cox and Ruming (2004) and Micklethwaite and Cox (2004) related clusters of gold deposits in the Eastern Goldfields Province to either dilational or—in contrast to Weinberg et al. (2004)—contractional jogs along seismically active shear zones. In their scenario, jogs in seismically active zones provide particularly favourable locations for gold mineralization because they tend to arrest fault movement and, by consequence, tend to localize aftershock activity within lobate domains surrounding the jogs that localized repeated rupture arrest. Unlike major seismic events, aftershocks are distributed over a wide area and give rise to long-lasting (orders of years to several decades), seismically

Fig. 6 Yilgarn gravity gradients derived by upward continuation to 60 km and coloured by height (*blue*, fine scale; *red*, coarse scale) and the location of gold deposits (*black dots*). Major deposits are labelled



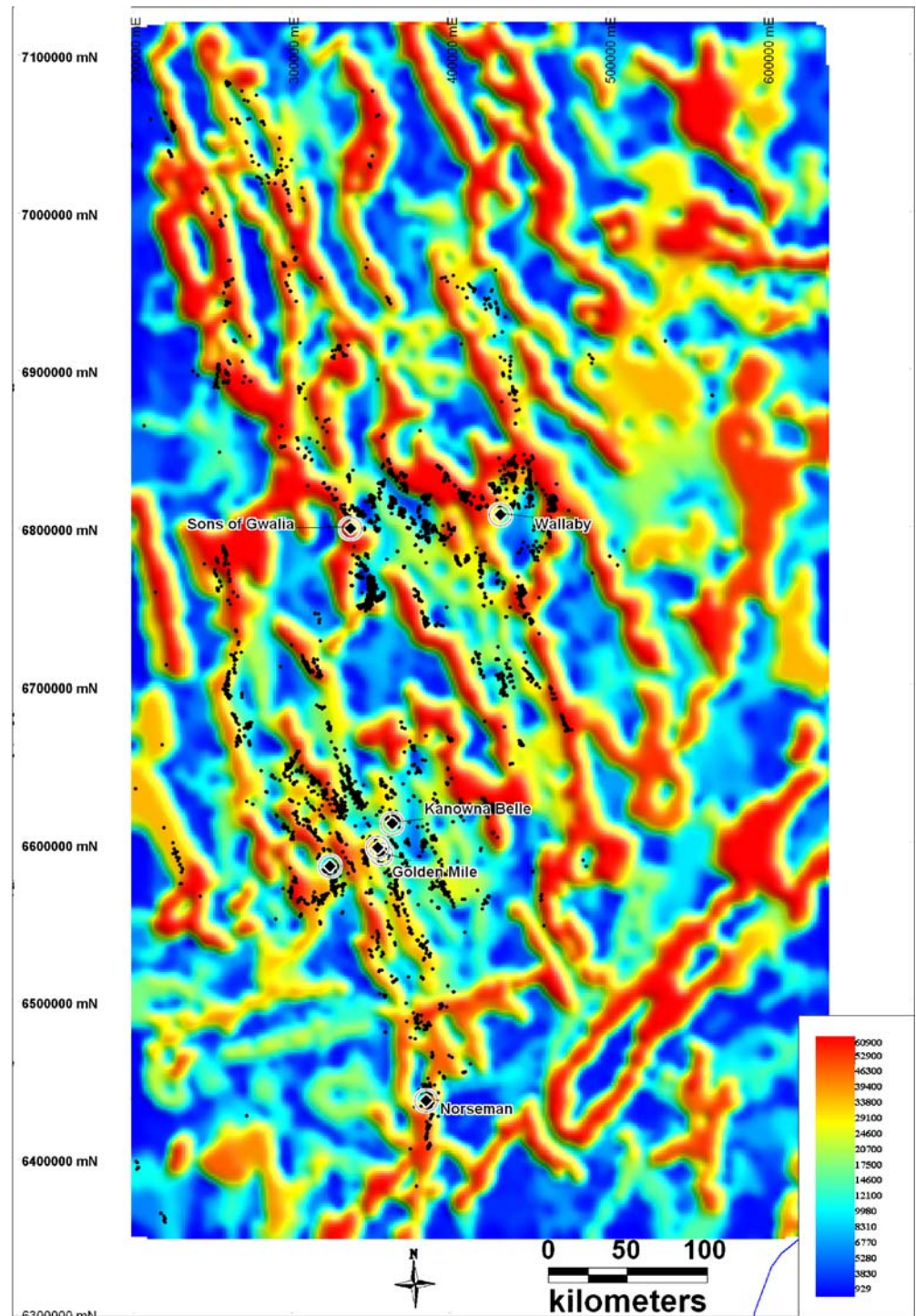
maintained zones of high permeability. Areas as far as 5–10 km from fault jogs would undergo repeated aftershock events and induce gold deposition through fluid flow focusing.

An example of contrasting interpretations is the St. Ives gold camp, which Weinberg et al. (2004) suggested is related to a large-scale extensional jog to the south of the gold deposits, whereas Cox and Ruming (2004) suggested that the same camp resulted from aftershocks related to the smaller-scale (i.e., kilometer) contractional jog within the gold camp. The Cox and Ruming (2004) model provides a more satisfactory explanation of the clustering of gold

occurrences in the Yilgarn Craton along low-displacement faults and shear zones, consistent with actualistic knowledge of how permeability is created in contemporary seismogenically active systems (S. Cox, personal communication, 2005).

Clearly, gold deposit location is controlled by the interaction of numerous factors that were active across many scales. A certain feature that may be important in focusing fluid flow at a broad scale, such as dilation, might neither be present nor important at a smaller scale. It is possible that these two apparently mutually exclusive

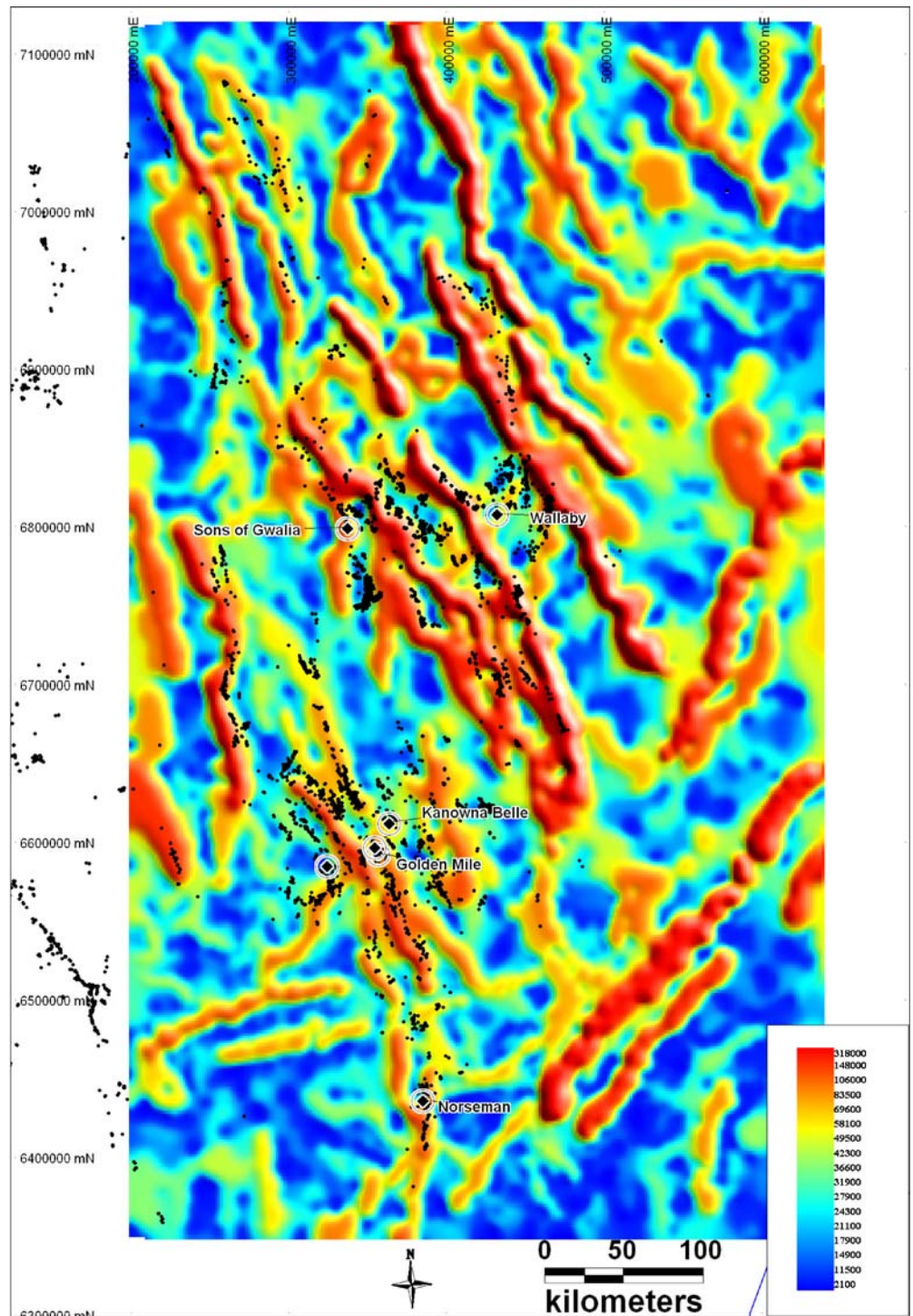
Fig. 7 2.5-D representation of height-weighted gravity gradients and gold deposits with major deposits labelled. *Warmer colours* represent height-persistent (more penetrative) edges



conclusions represent a reflection of different controls on fluid flow at different scales. Although we agree, in principle, that jogs in seismically active shear zones arrest fault movement and repetitive aftershocks have the ability to focus fluid, we suggest that the intrinsic increase in porosity and permeability in dilation regions should naturally favour fluid flow into these areas. Consequently, one could argue that these zones should preferentially host large deposits, whereas the opposite might be true for contractional jogs. On the other hand, there is no inherent

reason why a dilational jog zone should be more permeable than a contractional jog zone. Both structures essentially are sites of high damage intensity and potentially high fluid flux. The Victory Complex in the St. Ives goldfield is an excellent example of a mineralized contractional jog that is characterized by extreme dilation and brecciation along many of its component faults and shears (S. Cox, personal communication, 2005). Nonetheless, we argue that faults should have a greater potential to efficiently focus fluid flow that leads to mineralization compared to simple

Fig. 8 2.5-D representation of length-weighted gravity gradients and gold deposits with major deposits labelled. *Warmer colours* represent more strike-continuous edges



tension gashes. This is because faults tend to have a larger catchment as they grow with movement. Also, faults impose significant stress changes and strain rate variations in their surroundings that further increase the extent of damage zones. Therefore, dilational faults should naturally be more favourable than simple dilational cracks. However,

even though dilational cracks might not play a significant regional-scale role in focusing fluids, if such dilational cracks develop along fluid paths, they may provide very effective sites for gold deposition in terms of a hydraulically connected network that is capable of draining fluid from large-volume reservoirs at depth.

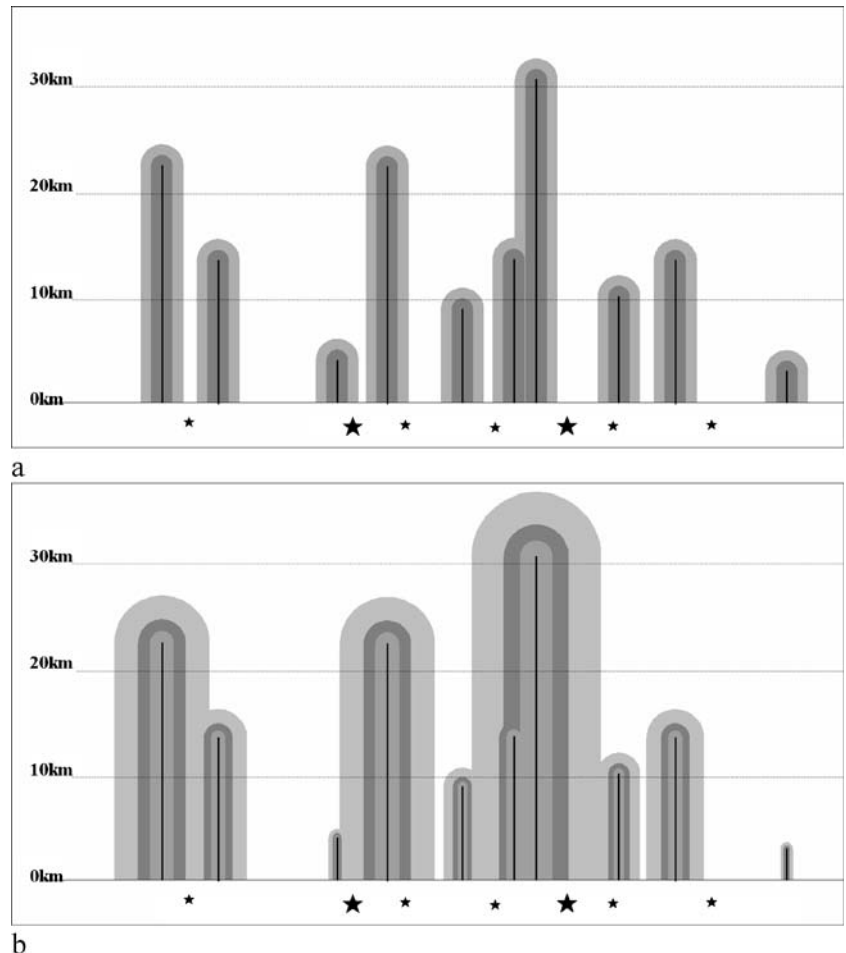
Spatial analysis of orogenic gold deposits, faults, and gravity gradients in the Yilgarn Craton

Scenario setting and methodology

Visual inspection of the distribution of deposits alone (see Fig. 2) indicates linear trends and some clustering. A spatial relationship of deposits to faults (Figs. 2 and 3) and gravity gradient edges (Fig. 6) is also apparent. Using these data sets and quantifying the empirical relationship between the gold occurrences and structural elements discussed above, we test possible scenarios that may influence the location of gold deposits. These tests involve determining the spatial relationship of deposits to:

1. Fold axial traces [examined in relation to regional anticlines (domes) and synclines (basins)]
2. Fault dimensions [Is there a correlation with fault length? Are small faults adjacent to large faults more mineralized than those further away from the influence of large faults?]
3. Fault trends and intersections [bends (i.e., a change in strike direction between 15° and 45°) and jogs (offset of faults at $>45^\circ$), and intersections with other structures (e.g., faults)]
4. Gravity gradient dimensions [Is there a correlation with the dimensions (length/height) of gravity gradients?]

Fig. 9 Example of buffer increments (shaded regions) around hypothetical faults (vertical black lines) of varying lengths (y-axis): **a** fixed-width buffers (1 and 2 km) and **b** variable-width buffers (a function of fault length). Stars on the x-axis represent positions of fictional deposits, sized according to the rank of the deposit



Geostatistical analysis of the proximity of surface point data (gold occurrences) to a range of vector lines (faults, folds and worms) and their associated parameters (e.g., length and height/depth), and examination of sensitivities of these parameters to total contained gold per unit area are used to evaluate the relationships. Buffer regions (i.e., subset areas) are created by surrounding vector lines, with one buffer made for all lines (rather than individual buffers per line). Successive buffer windows were created in an incremental fashion so as to capture the entire region of the data coverage.

The area (km^2) contained in each buffer increment and the total number of deposits in each tonnage group within each buffer increment are calculated, from which an 'endowment' value of metal content per unit area is derived. Appropriate buffer window sizes are selected with care because they can be made too small or too large to be meaningful in relation to data distribution. Two approaches were taken (Fig. 9) to address this concern. One approach is where the buffer size has a fixed distance (e.g., 1 and 2 km) from the vector line and is essentially independent of individual fault or gravity gradient size. The second approach is where the buffer size is a function of the inherent parameters of the fault or gravity gradient (e.g., length and height). There is a variable distance of the buffer from the vector, within a range defined by the minimum

and maximum values of the embedded vector parameter. In the first method, all vectors have similar areal influence, whereas in the second method, longer (or deeper/higher) features are weighted compared to short vectors. This has the effect that large dimension features will have a greater spatial influence. This has a reasonable geological basis in relation to fault growth models that show, in general, an increasing damage zone width with increased displacement (e.g., Childs et al. 1996).

For the analysis of bends, jogs and intersections, an automated routine, called Spatial Data Modelling (MapInfo; Avatra Geosystems 2004), was used. Fault bends are based on recognizing a change in strike direction of between 15° and 45° along an individual fault trace. Fault jogs are based on separation between fault terminations where a line that would pin the two faults is >45° from the strike of the individual fault strands.

Results and interpretation

In test 1, to examine the importance of fold axial traces, regional-scale anticlines and synclines were buffered at 5-, 10-, 20- and 40-km distances and the distribution of gold occurrences within these intervals was compared. Different slopes in the distributions indicate that anticlines (or domes) are generally more mineralized than synclines (or keels; Fig. 10a). This closure geometry is evidently a better trap or focus for mineralizing fluids.

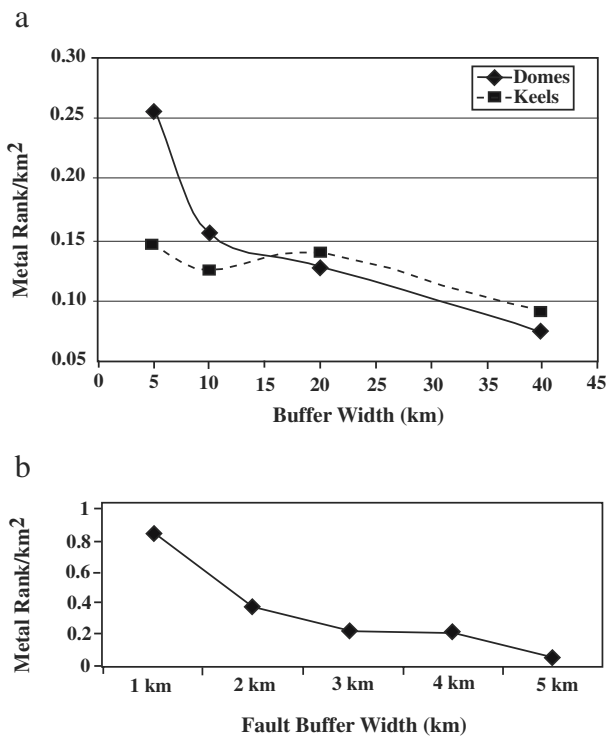


Fig. 10 **a** Distribution of mineralization (metal rank per km²) in buffers of varying distances from antiforms (*domes*) and synforms (*keels*). **b** Distribution of mineralization (metal rank per km²) in buffers of varying distances from faults for 1-, 2-, 3-, 5- and 10-km buffer widths

Examination of fault dimensions during test 2, using fixed-width buffer intervals and calculating gold per unit area within each interval (Fig. 10b), shows a slope that indicates increased gold content in buffers that are more proximal to faults, confirming visual assessment (Fig. 2). Fault population was then partitioned into length groupings defined by upper size limits (i.e., <20, <40, <60, <80 and <100 km) and a 2-km-wide buffer applied to each group. There is a gradual decrease in endowment as the overall fault length increases (Fig. 11a). This is interpreted to suggest that smaller faults (<20 km) are generally more mineralized than longer ones. Similarly, by subsetting the fault length as a series of ranges (i.e., <5, 5–10 and 10–25 km) and by applying 1- and 2-km fixed-width buffers to each length category (Fig. 11b), there is an overall increase in metal endowment for the shorter strikelength faults and a slight increase (or spike) in those with 25- to 50-km lengths.

To investigate if mineralization is related to small faults that are close to large faults, two separate scenarios were evaluated in the context of test 2. In the first instance, faults

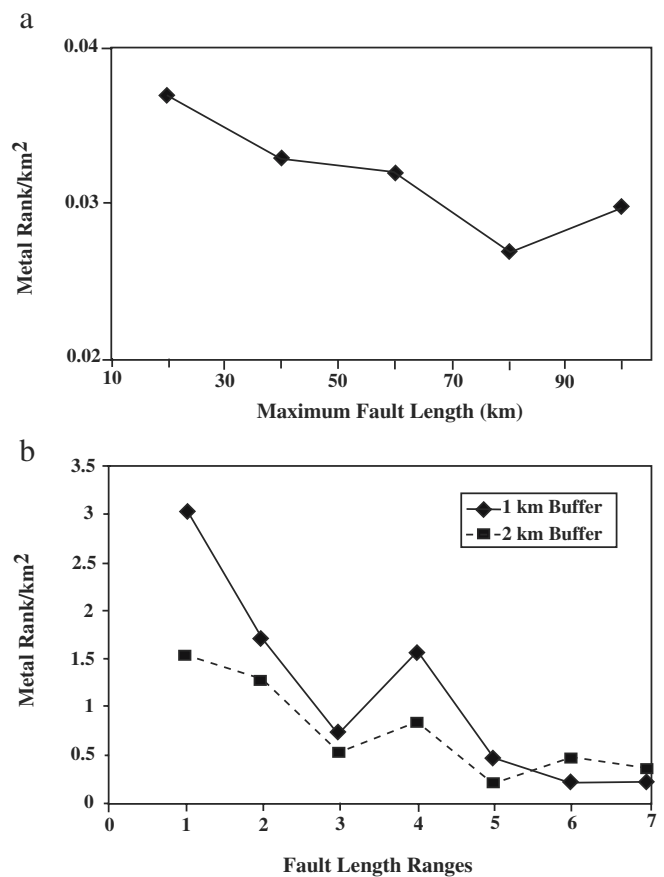


Fig. 11 **a** Distribution of mineralization (metal rank per km²) in 2-km buffer areas from faults that are subsampled into length ranges defined by upper maxima (e.g., <20 and <40 km). **b** Distribution of mineralization (metal rank per km²) in fixed-width (1 and 2 km) buffer areas from faults that are subsampled into length ranges defined by upper and lower values ('windows') where 1 1–5 km, 2 5–10 km, 3 10–25 km, 4 25–50 km, 5 50–100 km, 6 100–250 km, 7 >250 km. Diamond symbols, 1 km; square symbols, 2 km

>100-km-long were buffered to 4-km width. Gold occurrences surrounding faults that are partially or entirely within these larger fault envelopes were compared to those surrounding faults entirely outside of large fault envelopes. The total mineralization measured by rank (i.e., tonnage group) is not significantly different between the areas inside (0.09 per km^2) and outside (0.08 per km^2) the large fault buffers, whereas the total mineralization measured by production is significantly different, with 130 kg per km^2 gold contained inside vs 30 kg per km^2 for outside large fault envelopes. These results suggest that faults proximal to larger fault corridors are, on average, better endowed than those that are unrelated to large faults. In the second of these scenarios within test 2, a series of regions where the buffer width is a variable of fault length was created (e.g., Sunrise Dam region; Fig. 12). Notably, each buffer window represents a range of widths, depending on the individual length of the fault. The abundance of ranked mineral deposits within each buffer window was then calculated, using the maximum buffer width to represent each range. The resulting slope yields an increase in abundance with proximity to length-weighted faults and suggests a power law control (not shown). This mirrors non-weighted analysis (Fig. 11). Significantly, however, metal endowment is considerably higher per unit area for the more proximal buffer areas in the length-weighted analysis, suggesting that fault length plays a major role in engendering endowment.

The fixed-width and variable-width buffer results, described above, may be combined by taking a maximum value for the range of each buffer width increment in the length-weighted analysis (defined by the longest fault) and by plotting this with fixed-width data (Fig. 13a). Whereas both show an increase in metal tonnage with proximity to faults, changes in the slope of the distributions indicate a greater endowment per unit area with proximity to long

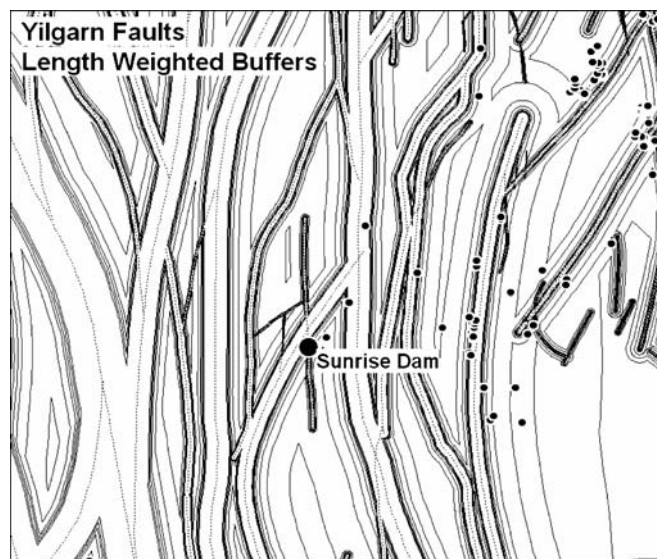


Fig. 12 Map of faults (dashed lines) and length-weighted buffers (solid lines) and deposits (dots) for the Sunrise Dam region. Note that small faults have narrow buffers, whereas long faults have wide buffers

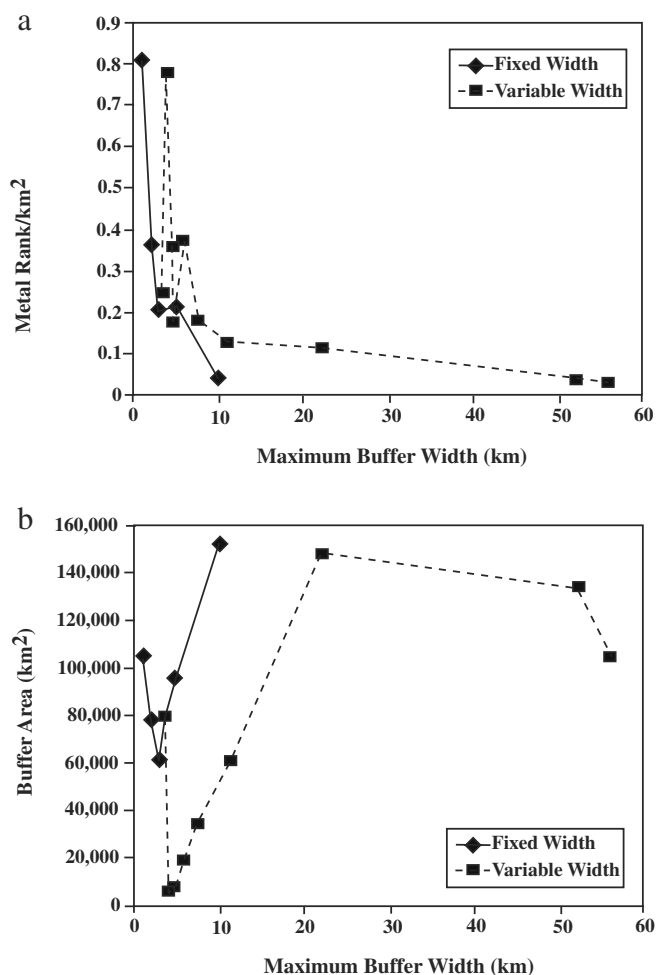


Fig. 13 Comparison of fixed-width and variable-width (weighted by length parameter) fault buffer methods for **a** metal endowment and **b** buffer sizes (km^2). The x-axis represents the maximum width of the buffer for the longest fault in the population, and narrow buffers are more proximal to the fault (i.e., 140 km is a proximal or narrow buffer; 5 km is a distal buffer)

strikelength faults. For example, for a maximum buffer width of 10 km, the endowment contained in variable-distance buffers is ten times that of the fixed distance buffers. Thus, although small faults are evidently important in hosting gold (Fig. 11a), an underlying control on ore is likely the presence of large-dimension (i.e., first-order) faults in the region. The exploration significance of this observation becomes more apparent by comparing the aerial size of buffers, or effective search areas, for the two methods (Fig. 13b). Importantly, the size of the search region is reduced by an order of magnitude using fault length as an area selection filter. For example, for a maximum buffer width of 5 km, the search areas of fixed buffers compared with variable buffers are approximately $100,000$ and $20,000 \text{ km}^2$, respectively (Fig. 13b). This, combined with increased endowment (Fig. 13a), is a potentially powerful area selection filter for exploration.

For test 3, bends and jogs were located and buffered at 2-km intervals. Several variations of bends and jogs were assessed, suggesting that bends appear slightly better

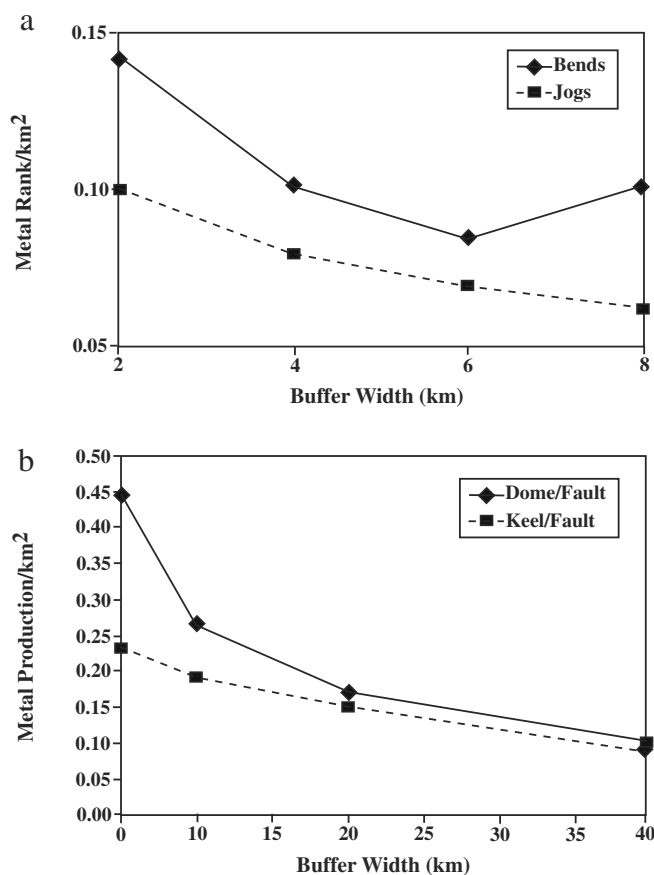


Fig. 14 **a** Relationship of mineralization to jogs and bends shown for differing buffer widths (2, 4, 6 and 8 km). Endowment decreases with increasing buffer width. **b** Relationship of mineralization to intersections of major faults (>100 km length) and regional fold axes (domes, anticlines; keels, synclines); fold buffer widths: 1 5 km, 2 10 km, 3 20 km, 4 40 km. The fault buffer width is constant at 2 km

endowed than jogs (Fig. 14a). Intersections of major fault buffers and buffered anticlines and synclines were also assessed. In this case, gold endowment is clearly higher at intersections of anticlines with major faults than at intersections of synclines with major faults. In both cases, gold tonnage at the intersection is also greater than that along individual faults or fold axes in isolation (Fig. 14b). Table 1 shows the various fault-related and fold-related factors analysed in this study in terms of both ranked occurrence and production. Overall, the best endowment from these tests appears to be associated with intersections of faults with anticlines and with small faults in relative proximity to larger structures. Significantly more production is related to jogs and small faults near large faults.

Visual inspection of Figs. 6, 7 and 8 suggests a spatial correlation between metal distributions and gravity gradient sheets and their derived values of edge length and height persistence. This is evident on district-scale gravity gradient maps for the five largest gold deposits or camps in the Eastern Goldfields (Figs. 15, 16 and 17). Spatial correlations are seen between gold distributions and coarse-scale edges, but this relationship does not hold

Table 1 Relative gold endowment associated with various factors that are included in the GIS analysis discussed in this study; *mineralization rank* is given as the sum of ranked occurrences per unit area, whereas *mineralization production* is the sum of Au production (in kg) per unit area

| Factor | Mineralization rank | Mineralization production |
|--------------------------------------|---------------------|---------------------------|
| Average for the whole Yilgarn Craton | 0.01 | 5 |
| Major fault >100 km | 0.04 | 18 |
| Small faults away from major faults | 0.08 | 30 |
| Long gravity gradients | 0.05 | 34 |
| Synclines | 0.14 | 44 |
| Anticlines | 0.26 | 67 |
| Intersection syncline, major fault | 0.23 | 120 |
| Small faults near major faults | 0.09 | 130 |
| Bends, all faults | 0.10 | 173 |
| Jogs, all faults | 0.14 | 340 |
| Intersection anticline, major fault | 0.45 | 430 |

true for all gold occurrences. To quantify this during test 4, gravity gradient vectors that lie within a 10-km radius of the largest five deposits are characterized by length and height variables (log/log plots; Fig. 18). The resulting graphs show a range of distributions, yet all indicate the presence of penetrative (long/deep) edges in search area and some have a higher density of shallow features (e.g. Wallaby, Norseman).

A regional-scale analysis of the vectorized gravity gradients was undertaken using the variable-width buffering approach, introduced above, and the buffers weighted for vector height (Fig. 7) and length (Fig. 8), respectively. In the former, there is a gradual increase in gold tonnage with proximity to height-weighted gravity gradients, and this decreases for the most proximal buffer (Fig. 19a). The decrease may be a function of the sampling method and/or the scale of the data. However, the increase in slope with proximity to coarse-scale gravity gradient is a real effect. This is observed in tandem with a decreasing search area and smaller maximum buffer widths (Fig. 19b). Length-weighted plots show a broadly similar pattern (Fig. 20a,b) to the height-weighted ones. The inference drawn from this is that the distribution of gold is strongly correlated with proximity to long/deep gravity gradients, but need not be positioned immediately adjacent to such gradients. This is consistent with the interpretation derived from the fault analysis that small faults adjacent to large faults are more prone to be mineralized. Whereas this is not a surprising result in terms of empirical exploration parameters and is consistent with previous studies (e.g., Knox-Robinson 2000; Weinberg et al. 2004), quantitatively applying this in an exploration program may be critical for success. The reduction in search area by applying these parameters has a

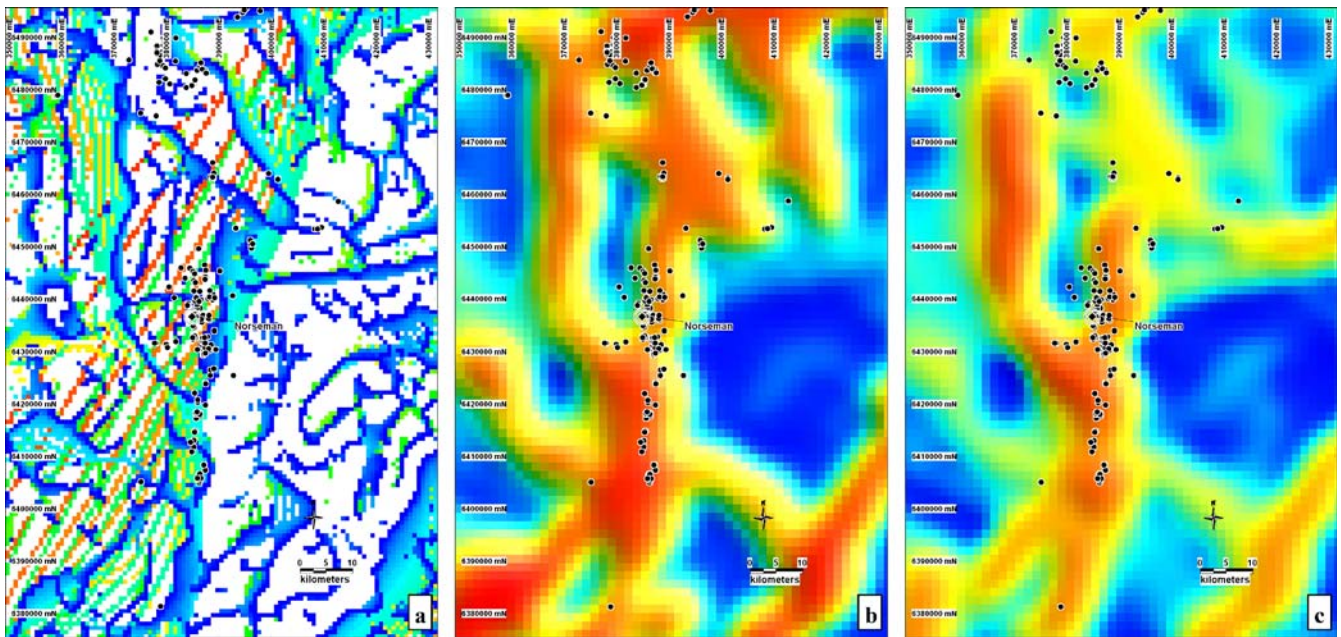


Fig. 15 Norseman region: **a** gravity gradient distribution, **b** interpreted height-weighted images and **c** length-weighted images. Colour scales in this figure and in Figs. 16 and 17 are as in Figs. 6, 7 and 8, respectively

significant impact on area selection decisions, particularly when using gravity in regions under cover.

Discussion and conclusions

Recent advances in the acquisition, processing and integration of large and diverse data sets have enabled mineral explorationists to increasingly apply computer-based and conceptual strategies that can augment and significantly enhance a mainly field-based empirical approach. This has led to the development of a variety of techniques that use knowledge-driven and/or data-driven approaches to efficiently extract exploration-relevant factors from multidisciplinary data sets, and that integrate these into mineral prospectivity maps at the local to regional scales (e.g., An et al. 1991; Bonham-Carter 1994; Gong 1996; Knox-Robinson 2000). Several studies have illustrated the use of GIS as an efficient tool for conceptual mineral exploration in areas of the Australian continent that are characterized by poor exposure, such as the Yilgarn Craton, Lennard Shelf, Pine Creek Inlier and southern New England Orogen (e.g., Wyborn et al. 1994; Knox-Robinson and Groves 1997; Brown et al. 2000; D'Ercole et al. 2000; Gardoll et al. 2000). These studies variably considered lithology, metamorphic grade, major structures, geometry of geological bodies, geophysical criteria and spatial relationships to construct prospectivity maps at the camp to regional scale. Prospectivity analyses in these studies were mainly based on the coincidence of empirically based, diagnostic and permissive criteria (weights-of-evidence), and the use of artificial neural networks that employ pattern recognition and classification via the simultaneous analysis of all input parameters. In contrast to the approach used in these studies, the strength of prospectivity assessment in

this investigation lies in the regional-scale to terrane-scale integration and utilization of easily accessible parameters. These methods seek to quantify the empirical spatial relationship between orogenic gold deposit, faults and potential field gradients and to define critical parameters that are likely to determine the location and size of deposits along prospective structures.

Fault control on gold deposit localization in the Yilgarn Craton is manifest, but is just one piece of the puzzle to unravelling concepts on gold genesis and deposition. 'Fertile' or prospective positions along fault systems, in general, are commonly those with a perceived increased fracture intensity, permeability and (or) roughness. These may include dilational relay ramps and jogs, cross-faults and areas of maximum displacement, reactivation and postseismic failure (e.g., Zhang et al. 2001; Betts and Lister 2002; Cox and Ruming 2004). Additional factors, well-known to explorationists in the Yilgarn Craton, include: proximity to crustal-scale faults, regional anticlinal hinge zones, strike changes, strong rheological contrasts and metamorphic grades. A characteristic spacing of large deposits along major faults is also apparent, at least in the case of the Boulder-Lefroy Shear Zone (Weinberg et al. 2004).

Metallogenically important major faults are commonly steep and possibly translithospheric, as demonstrated by a close spatial association of mantle-derived magmas along many of these structures (Rock et al. 1990; Bierlein et al. 2001). On the other hand, a listric geometry has implications for their capability to transect the lithosphere and access potential fluid/heat reservoirs in the mantle. The demonstrated association between significant potential field (gravity) gradients and gold distribution in the Yilgarn Craton confirms the spatial link between orogenic gold deposits and deep-seated major faults. Seismic surveys

Fig. 16 Wallaby–Sons of Gwalia region: **a** gravity gradient distribution, **b** interpreted height-weighted images and **c** interpreted length-weighted images

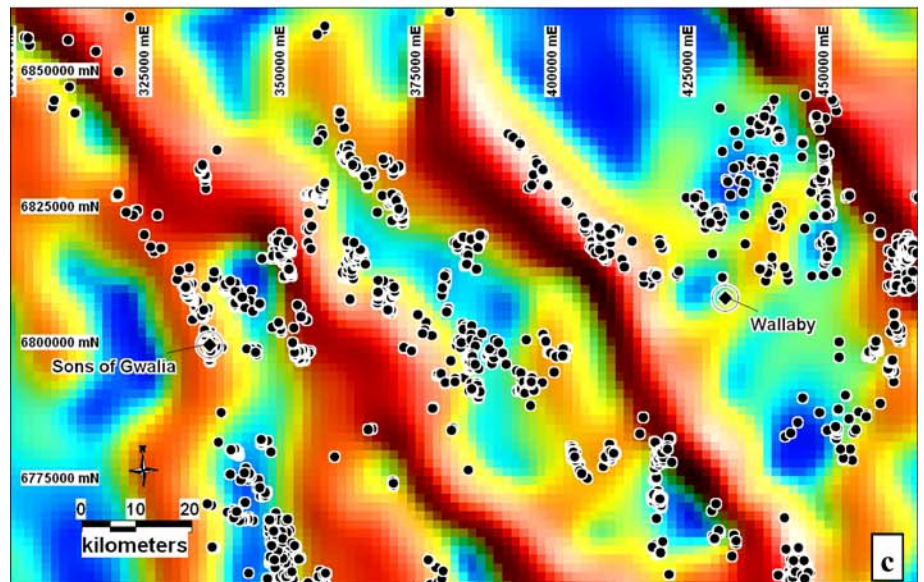
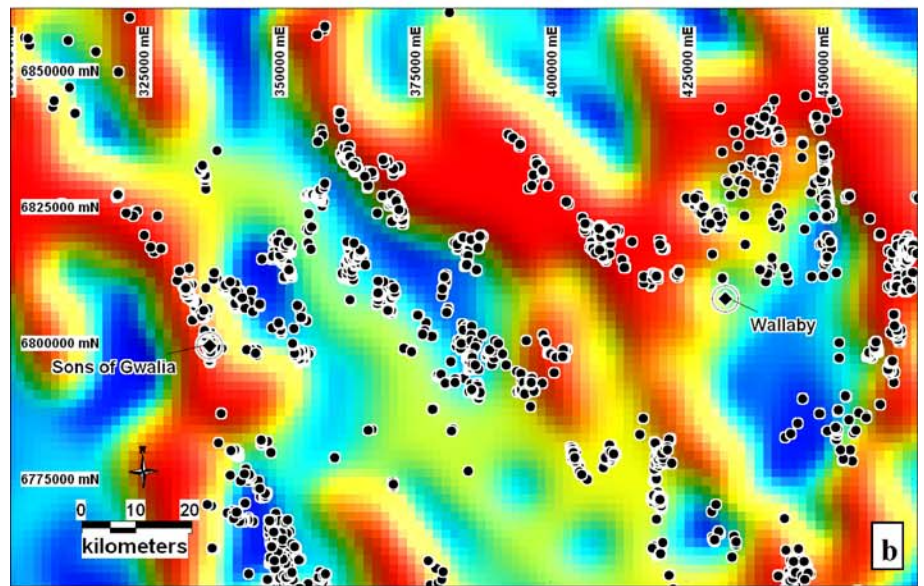
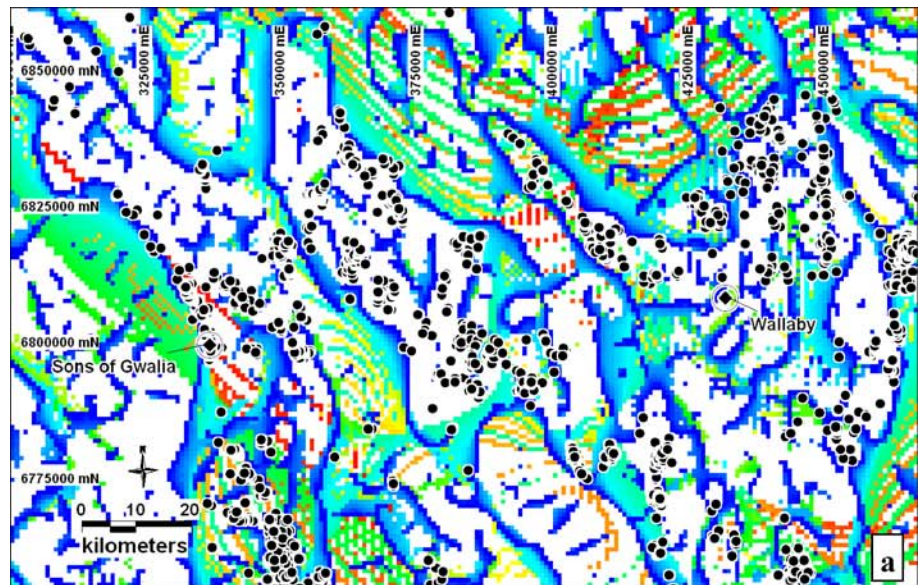
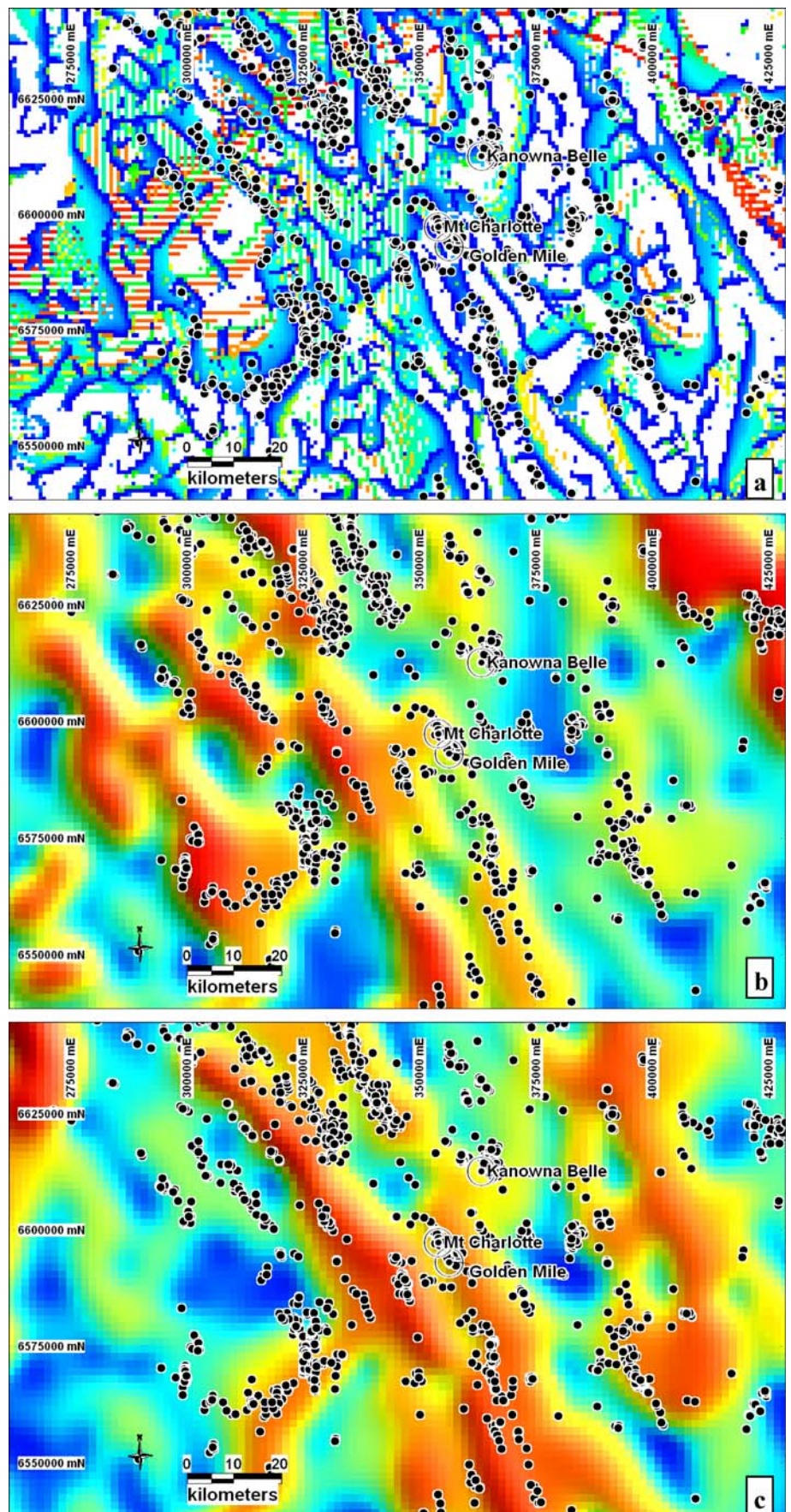


Fig. 17 Golden Mile–Kanowna Belle region: **a** gravity gradient distribution, **b** interpreted height-weighted images and **c** interpreted length-weighted images



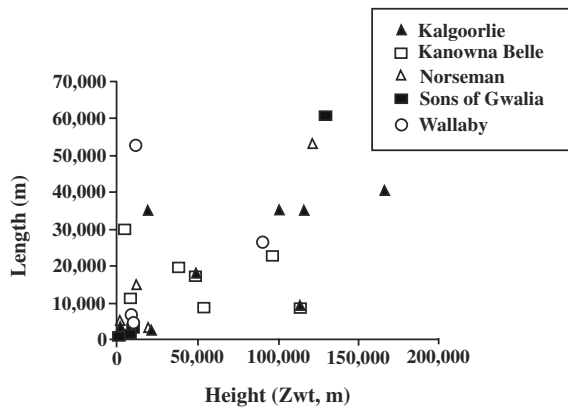


Fig. 18 Scatter plot of height (z_{wt} , in meters) vs length (in meters) for gravity vector gradient distributions within the 10-km radius of major gold deposits (>100,000 kg) in the Eastern Goldfields Province

reveal that many of the steep faults in the eastern Yilgarn Craton are listric and merge with a flat-lying reflector lower in the crust (e.g., Goleby et al. 2004). Therefore, large-dimension edges seem to provide a reliable first-order area selection filter for exploration, particularly in areas of poor exposure.

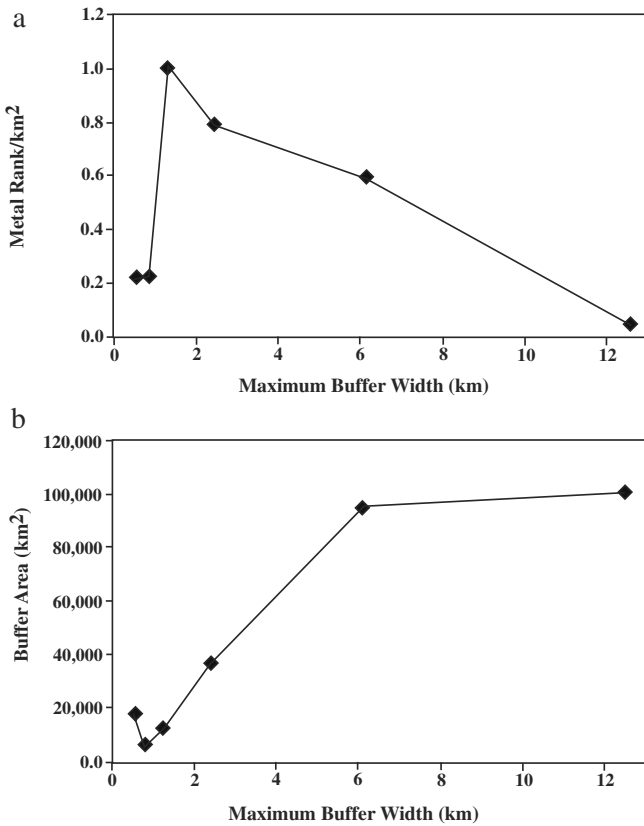


Fig. 19 **a** Distribution of mineralization (metal rank per km^2) in variable-width gravity gradient buffers that are weighted by upward migration height parameter (z_{wt}). The x -axis represents the maximum width of the buffer for the highest gradient in the population, and narrow buffers are more proximal to the gradient. **b** Plot of area (in km^2) of each successive buffer increment against the maximum buffer width (in km) per increment

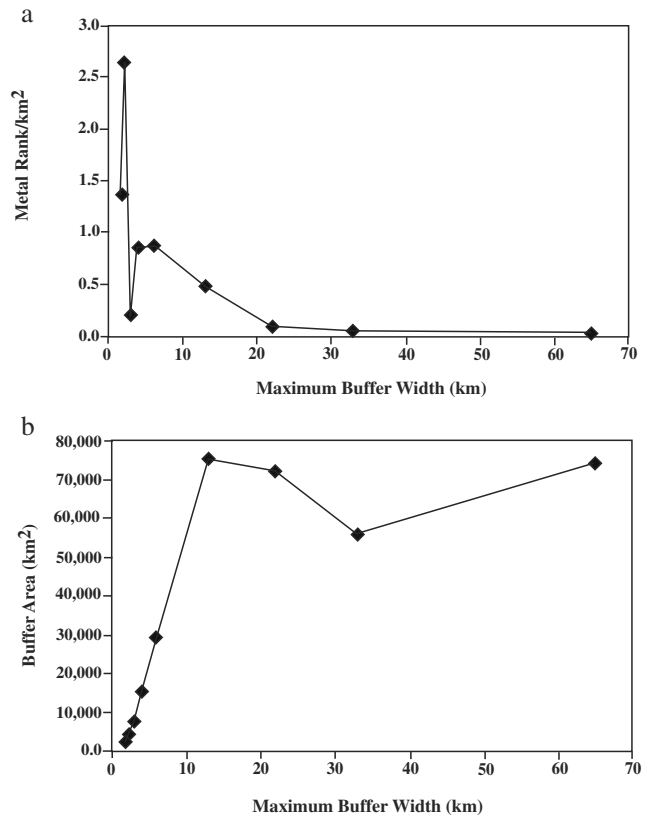


Fig. 20 **a** Distribution of mineralization (metal rank per km^2) in variable-width gravity gradient buffers that are weighted by strike-length parameter. The x -axis represents the maximum width of the buffer for the longest gradient in the population, and narrow buffers are more proximal to the gradient. **b** Plot of area (in km^2) of each successive buffer increment against the maximum buffer width (in km) per increment

Reduction of the exploration search area is a consequence of applying straightforward probability tests on relatively accessible and easily measured parameters. These show that endowment can be correlated with the intersections of anticlines and major faults. In particular, we find that gold is preferentially associated with smaller (second-order and third-order) faults that are within close proximity of major (first-order) faults. The recognition that major faults are important is not new, nor is the observation that small faults preferentially host the gold (e.g., Groves et al. 1998). However, it is the combination of small faults under the influence of long strike-length faults that seems to be the key in understanding where orogenic gold is preferentially distributed. It is pertinent to note that similar controls are indicated for Palaeozoic volcanic-hosted massive sulfide deposits in western Tasmania (Murphy et al. 2004). Penetrative structures provide pathways for metal transport or create suitable geometries for stress-driven fluid flow, and these fluids migrate or diffuse away from large faults to depositional sites along smaller faults. There is a strong permeability control on orogenic gold distribution, consistent with major fault growth episodes ('golden aftershocks' of Cox and Ruming 2004).

The analysis used here indicates that a systematic approach in integrating regional data sets can have a practical application to defining exploration targeting criteria. In particular, applying these criteria may have some advantages over approaches that use Boolean logic (i.e., prospective/non-prospective; e.g., Knox-Robinson 2000) in that they allow for the distinction between multiple degrees of prospectivity, or 'fertility'. Further work is needed to take the predominantly regional-scale parameters in this study and apply them at the prospective scales.

Acknowledgements This study was conducted as part of the predictive mineral discovery Cooperative Research Centre (pmd*CR) and is published with the permission of the CEO of pmd*CR. We are grateful to the following people for input into this study: R. Korsch, B. Goleby, B. Drummond, I. Roy, A. Barnicoat (Geoscience Australia); G. Hall, S. Halley, G. Tripp (Placer Dome); F. Robert (Barrick Australia); R. Smith, C. Swaager (AngloGold); G. Begg, J. Hronsky (WMC); N. Archibald (Geoinformatics); I. Vos, A. Morey, P. Betts, C. Janka (Monash University); T. Blenkinsop (James Cook University); R. Woodcock, A. Ord, P. Roberts, A. Dent, S. Cox, J. Walshe, S. Fraser (CSIRO); S.F. Cox (ANU); D. Groves (University of Western Australia); B. Hobbs (Department of Premier and Cabinet, WA); and R. Goldfarb (US Geological Survey). The gravity gradients used in this study were generated by Fractal Graphics (now Geoinformatics). We thank Juhani Ojala, Warwick Brown and Richard Goldfarb for their constructive reviews. This is TSRC publication number 340.

References

- An P, Moon WM, Rencz AN (1991) Application of fuzzy set theory to integrated mineral exploration. *Can J Explor Geophys* 27:1–11
- Archibald NJ, Gow P, Boschetti F (1999) Multiscale edge analysis of potential field data. *Explor Geophys* 30:38–44
- Archibald NJ, Holden D, Mason R, Power B, Boschetti F, Horowitz F, Hornby P (2001) There's a worm in my soup: wavelet based analysis for interpretation of crustal scale potential field data and implications for identification of giant hydrothermal ore systems. In: 2001—a hydrothermal odyssey, Townsville, EGRU, James Cook University, Queensland, pp 5–7
- Avantra Geosystems (2004) MapInfo Spatial Data Modelling Tool (MI-SDM v1.85), Avantra Geosystems. <http://www.avantra.com.au>
- Betts PG, Lister GS (2002) Geodynamically indicated targeting strategy for shale-hosted massive sulfide Pb–Zn–Ag mineralisation in the Western Fold Belt, Mt. Isa terrane. *Aust J Earth Sci* 49:985–1010
- Betts PG, Giles D, Lister GS (2004) Aeromagnetic patterns of half-graben and basin inversion: implications for sediment-hosted massive sulphide Pb–Zn–Ag mineralisation. *J Struct Geol* 26:1137–1156
- Bierlein FP, Hughes M, Dunphy J, McKnight S, Reynolds PR, Waldron HM (2001) Trace element geochemistry, $^{40}\text{Ar}/^{39}\text{Ar}$ ages, Sm–Nd systematics and tectonic implications of mafic–intermediate dykes associated with orogenic lode gold mineralisation in central Victoria, Australia. *Lithos* 58:1–31
- Blenkinsop T, Bierlein FP (2004) Fault roughness and mineral endowment; a fractal approach. 4th International conference on fractals and dynamic systems in geoscience, Technische Universität, München, Germany, 19–22 May, pp 6–9
- Bonham-Carter GF (1994) Geographic information systems for geoscientists: modelling with GIS. Computer methods in the geosciences, vol 13. Pergamon, New York
- Brown WM, Gedeon D, Groves DI, Barnes RG (2000) Artificial neural networks: a new method for mineral prospectivity mapping. *Aust J Earth Sci* 47:757–770
- Chernicoff CJ, Richards JP, Zappettini EO (2002) Crustal lineament control on magmatism and mineralization in northwestern Argentina: geological, geophysical, and remote sensing evidence. *Ore Geol Rev* 21:127–155
- Childs C, Watterson J, Walsh JJ (1996) A model for the structure and development of fault zones. *J Geol Soc Lond* 153:337–340
- Cowie PA, Scholz CH (1992) Displacement–length scaling relationship for faults: data synthesis and discussion. *J Struct Geol* 14:1149–1156
- Cox SF, Ruming K (2004) The St. Ives mesothermal gold system, Western Australia—a case of golden aftershocks? *J Struct Geol* 26:1109–1125
- Cox SF, Knackstedt MA, Braun J (2001) Principles of structural control on permeability and fluid flow in hydrothermal systems. *Soc Econ Geol Rev* 14:1–24
- Crafford AEJ, Grauch VJS (2002) Geologic and geophysical evidence for the influence of deep crustal structures on Paleozoic tectonics and the alignment of world-class gold deposits, north-central Nevada, USA. *Ore Geol Rev* 21:157–184
- D'Ercole CD, Groves DI, Knox-Robinson CM (2000) Using fuzzy logic in a geographic information system environment to enhance conceptually based prospectivity analysis of Mississippi Valley-type mineralisation. *Aust J Earth Sci* 47:913–927
- Drummond BJ, Goleby BR, Goncharov AG, Wyborn LAI, Collins CDN, MacCready T (1998) Crustal-scale structures in the Proterozoic Mount Isa Inlier of north Australia: their seismic response and influence on mineralisation. *Tectonophysics* 288:43–56
- Ewers GR, Evans N, Kilgour B (compiler) (2002a) MINLOC Mineral Localities Database [digital data set]. Geoscience Australia, Canberra. http://www.ga.gov.au/general/technotes/20011023_32.jsp (cited April 2003)
- Ewers GR, Evans N, Hazell M, Kilgour B (compiler) (2002b) OZMIN Mineral Deposits Database [digital data set]. Geoscience Australia, Canberra. http://www.ga.gov.au/general/technotes/20011023_32.jsp (cited April 2003)
- Gardoll SJ, Groves DI, Knox-Robinson CM, Yun GY, Elliott N (2000) Developing the tools for geological shape analysis, with regional- to local-scale examples from the Kalgoorlie Terrane of Western Australia. *Aust J Earth Sci* 47:943–953
- Goldfarb RJ, Groves DI, Gardoll S (2001) Orogenic gold and geologic time: a global synthesis. *Ore Geol Rev* 18:1–75
- Goleby BR, Korsch RJ, Fomin T, Bell B, Nicoll MG, Drummond BJ, Owen AJ (2002) Preliminary 3-D geological model of the Kalgoorlie region, Yilgarn Craton, Western Australia, based on deep seismic-reflection and potential-field data. *Aust J Earth Sci* 49:917–933
- Goleby BR, Blewett RS, Korsch RJ, Champion DC, Cassidy KF, Jones LEA, Groenewald PB, Henson P (2004) Deep seismic reflection profiling in the Archaean northeastern Yilgarn Craton, Western Australia: implications for crustal architecture and mineral potential. *Tectonophysics* 388:119–133
- Gong P (1996) Integrated analysis of spatial data from multiple sources: using evidential reasoning and artificial neural network techniques for geological mapping. *Photogramm Eng Remote Sensing* 62:513–523
- Grauch VJS, Rodriguez BD, Bankley V (2003) Evidence for a Battle Mountain–Eureka crustal fault zone, north-central Nevada, and its relation to Neoproterozoic–Early Paleozoic continental breakup. *J Geophys Res* 108(B3):2140
- Groves DI, Goldfarb RJ, Gebre-Mariam M, Hagemann SG, Robert F (1998) Orogenic gold deposits: a proposed classification in the context of their crustal distribution and relationship to other gold deposit types. *Ore Geol Rev* 13:7–27
- Groves DI, Goldfarb RJ, Knox-Robinson CM, Ojala J, Gardoll S, Yun GY, Holyland P (2000) Late-kinematic timing of orogenic gold deposits and significance for computer-based exploration techniques with emphasis on the Yilgarn Block, Western Australia. *Ore Geol Rev* 17:1–38

- Haynes DW (2002) Giant iron oxide–copper–gold deposits: are they in distinctive geological settings? In: Cooke DR, Pongratz J (eds) *Giant ore deposits: characteristics, genesis and exploration*, CODES Special Publication 4. Hobart, Tasmania, pp 57–77
- Hobbs BEH, Ord A, Archibald NJ, Walshe JL, Zhang Y, Brown M, Zhao C (2000) Geodynamic modelling as an exploration tool. In: *After 2000—the future of mining*, Sydney, pp 34–49
- Holden D, Archibald NJ, Boschetti F, Jessell, MW (2000) Inferring geological structures using wavelet-based multiscale edge analysis and forward models. *Explor Geophys* 31:617–621
- Holyland PW, Ojala VJ (1997) Computer-aided structural targeting in mineral exploration: two- and three-dimensional stress mapping. *Aust J Earth Sci* 44:421–432
- Hornby P, Boschetti F, Horowitz F (1999) Analysis of potential field data in the wavelet domain. *Geophys J Int* 137:175–196
- Jegouzo P (1980) The South Armorican shear zone. *J Struct Geol* 2:39–47
- Knox-Robinson CM (2000) Vectorial fuzzy logic: a novel technique for enhanced mineral prospectivity mapping with reference to the orogenic gold mineralisation potential of the Kalgoorlie Terrane, Western Australia. *Aust J Earth Sci* 47:929–941
- Knox-Robinson CM, Groves DI (1997) Gold prospectivity mapping using a Geographic Information System (GIS) with examples from the Yilgarn Block of Western Australia. *Chron Rech Min* 529:127–138
- Micklethwaite S, Cox SF (2004) Fault-segment rupture, aftershock-zone fluid flow, and mineralization. *Geology* 32:813–816
- Murphy FC, Denwer K, Keele R, Green G, Korsch R, Lees T (2004) Prospectivity analysis, Tasmania: where monsters lurk? *Aust Geol Soc Abstr* 73:102
- Myers JS (1995) The generation and assembly of an Archaean supercontinent: evidence from the Yilgarn Craton, Western Australia. In: Coward MP, Reis AC (eds), *Early Precambrian processes*, Geological Society Special Publication 95, pp 143–154
- O'Driscoll EST (1990) Lineament tectonics of Australian ore deposits. In: Hughes FE (ed), *Geology of mineral deposits of Australia and Papua New Guinea*. The Australian Institute of Mining and Metallurgy, Melbourne, pp 33–41
- Oliver NHS (2001) Linking of regional and local hydrothermal systems in the mid-crust by shearing and faulting. *Tectonophysics* 335:147–161
- Ord A, Hobbs BE (1989) The strength of the continental crust, detachment zones and the development of plastic instabilities. *Tectonophysics* 158:269–289
- Peacock DCP (2003) Propagation, interaction and linkage in normal fault systems. *Earth Sci Rev* 58:121–142
- Robert F, Poulsen KH (2001) Vein formation and deformation in greenstone gold deposits. *Soc Econ Geol Rev* 14:111–155
- Rock NMS, Taylor WR, Perring CS (1990) Lamprophyres—what are lamprophyres? In: Ho SE, Groves DI, Bennett JM (eds), *Gold deposits of the Archaean Yilgarn Block, Western Australia: nature, genesis and exploration guides*. Geology Department and UWA Extension Publication 20, pp 128–135
- Russell MJ, Haszeldine RS (1992) Accounting for geofractures. In: Bowde AA, Earls G, O'Connor PG, Pyne JF (eds) *The Irish Minerals Industry 1980–1990*. Irish Association for Economic Geology, Dublin, pp 135–142
- Sibson RH (2001) Seismogenic framework for hydrothermal transport and ore deposition. *Soc Econ Geol Rev* 14:25–50
- Sillitoe RH (2000) Gold-rich porphyry deposits: descriptive and genetic models and their role in exploration and discovery. *Soc Econ Geol Rev* 13:315–345
- Stephens JR, Mair JL, Oliver NHS, Hart CJR, Baker T (2004) Structural and mechanical controls on intrusion-related deposits of the Tombstone Gold Belt, Yukon, Canada, with comparisons to other vein-hosted ore-deposit types. *J Struct Geol* 26:1025–1041
- Vos IMA, Bierlein FP, Murphy B, Barlow M (2004) The mineral potential of major fault systems: case studies from northeastern Queensland, Australia. In: Barnicoat AC, Korsch RJ (eds) *Geoscience Australia Record 2004/09*, pp 209–212
- Walker R, Jackson J (2002) Offset and evolution of the Gowk fault, SE Iran: a major intra-continental strike-slip system. *J Struct Geol* 24:1677–1698
- Weinberg RF, Hodkiewicz PF, Groves DI (2004) What controls gold distribution in Archean terranes? *Geology* 32:545–548
- Weinberg RF, van der Borgh P, Bateman RJ, Groves DI (2005) Kinematic history of the Boulder–Lefroy Shear Zone system and controls on associated gold mineralization, Yilgarn Craton, Western Australia. *Econ Geol* (in press)
- Wilde SA, Middleton MF, Evans BJ (1996) Terrane accretion in the southwestern Yilgarn Craton: evidence from a deep seismic crustal profile. *Precambrian Res* 78:179–196
- Wyborn LAI, Gallagher R, Mernagh T (1994) A conceptual approach to metallogenic modelling using GIS: examples from the Pine Creek Inlier. In: *Proceedings of a symposium on Australian research in ore genesis*, 12–14 December, Australian Mineral Foundation, Glenside, South Australia, pp 15.1–15.5
- Zhang Y, Hobbs BEH, Ord A, Walshe JL, Zhao C (2001) Interaction between faulting, deformation, fluid flow and mineral precipitation: a numerical modelling approach. In: *2001—a hydrothermal odyssey*, Townsville, EGRU, James Cook University, Queensland, pp 231–232